STUDIA UBB CHEMIA, LXIV, 2, Tom II, 2019 (p. 483-497)
(RECOMMENDED CITATION)
DOI:10.24193/subbchem.2019.2.41

Dedicated to Professor Ioan Bâldea on the Occasion of His 80th Anniversary

PROVENANCE STUDY ON A SMALL SELECTION OF ROMAN POTSHARDS (TĂŞNAD-SERE SITE, SATU MARE COUNTY, ROMANIA). II

ENIKŐ BITAY[a,d], BERNADETH KISS-PATAKI[b], EMIL INDREA[c], IRÉN KACSÓ[c], FERENC TOLVAY-ROŞCA[a], IOAN BRATU[c], ERZSÉBET VERESS[d*]

ABSTRACT. Characterization of five representative archaeological ceramic shards from the Tăşnad-Sere C 52 site by optical microscopy (OM), XRD, and FT-IR spectroscopy [1] was continued by the detailed analysis of the XRD and FT-IR spectroscopic data in order to obtain a deeper insight into the samples microstructure and mineral composition. The XRD investigations were also extended to several clayish soil samples collected in the archaeological site area. The fresh results permit more exact conclusions about the possible local provenance of the raw materials used by the ancient potters.

Keywords: *archaeological ceramics, provenance, XRD microstructure analysis, FT-IR spectra deconvolution*

INTRODUCTION

Earthenware is modelled (both manually or on potter's wheel) from "green" ceramic paste consisting of moist clays or (calcareous or siliceous) clayish soils, usually tempered with different additives. The "green" earthenware, after desiccation, is baked (sintered) in oxidative or reductive conditions. The highest baking (firing) temperatures possibly achieved in the pottering kilns used in the Roman Empire time were around 1100ºC. [2] During the firing, the tempered green clay paste metamorphoses, the mineral components of the

[a] *Sapientia Hungarian University of Transylvania, Faculty of Technical and Human Sciences, OP 9 CP 4, RO-540485 Târgu-Mureş, Romania*
[b] *Bosch Group in Hungary, Postbox 331, H-1475 Budapest Hungary*
[c] *National Institute for Research and Development of Isotopic and Molecular Technologies, Donath Str. 65-103, RO-400293 Cluj, Romania*
[d] *Transylvanian Museum Society, Napoca Str. 2-4, RO-400750 Cluj, Romania*
** Corresponding authors: ebitay@ms.sapientia.ro; veresserzsebet@gmail.com*

clayey matrix and the additives partly decompose, partly structurally rearrange below 950–1050ºC, forming the strengthened fired ceramic body.

Sintering supposes interactions at atomic and/or molecular level between the constituents of the green clay paste (matrix and temper) implying crystal deformation: the grain boundaries of the clay and temper crystallites start melting and/or re-crystallize. The process takes place via phase transition, resulting in the end a more compact material, the hardened bulk ceramic. Detailed data about the sintering processes (phase decomposition and/or transformation, structural changes of the inhomogeneous multiphase ceramic matrix during the firing) together with certain physical and technological parameters help to clarify the manufacturing method used by the ancient potters. [2] Similarities and differences in some properly selected characteristics of the investigated items (mineralogical and elemental composition, macro- and micro-structural issues) can lead to provenance-related conclusions as well. [3-5]

The XRD and FT-IR spectroscopic investigation of the sample selection formerly presented [1] was carried out with the aim to identify, among others, the sintering-induced vitrification and (re)crystallization processes occurred in - and the depositional changes suffered by - the ceramic shards taken for study. However, the capability of the archaeological ceramics' XRD diffractograms and FT-IR spectra to provide reliable information about the findings (their provenance, sintering conditions, the depositional processes suffered) is limited.

As on the XRD patterns appears (Fig. 1), the strong diffraction lines of quartz and feldspar frequently mask the presence of the minor clay minerals (pyroxenes, iron oxides); in addition, some XRD lines could be minimized due to the transformations occurred during firing or the deposition. [6] In fact, the “primary” XRD data allow only the semi-quantitative estimation of the principal mineral components [1] and the qualitative estimation of the structural ordering, and can't be even used to reliably identify all the (minor) mineral components present.

The FT-IR spectra of the samples published before {1} is dominated by the characteristic broad O–H bands of the ancient ceramics around 3400 and 1600 cm^{-1}, and the strong symmetry band centred at 1050 cm^{-1}, defined by the Si–O, Al–O and Si–O–Al units typically present in fired pottery, both constituted by the overlapped closely neighbouring peaks of the component clay minerals. Intensity and shape of the O–H bands depend, besides the firing conditions, on the deposition related rehydration and/or rehydroxylation, the latter being defined, at the same time, by the burial environment, ceramic composition and structure. The intensity and shape of the 1050 cm^{-1} band which characterizes the connectivity of the Si–O, Al–O and Si–O–Al units, is also defined by the ceramic composition and structure.

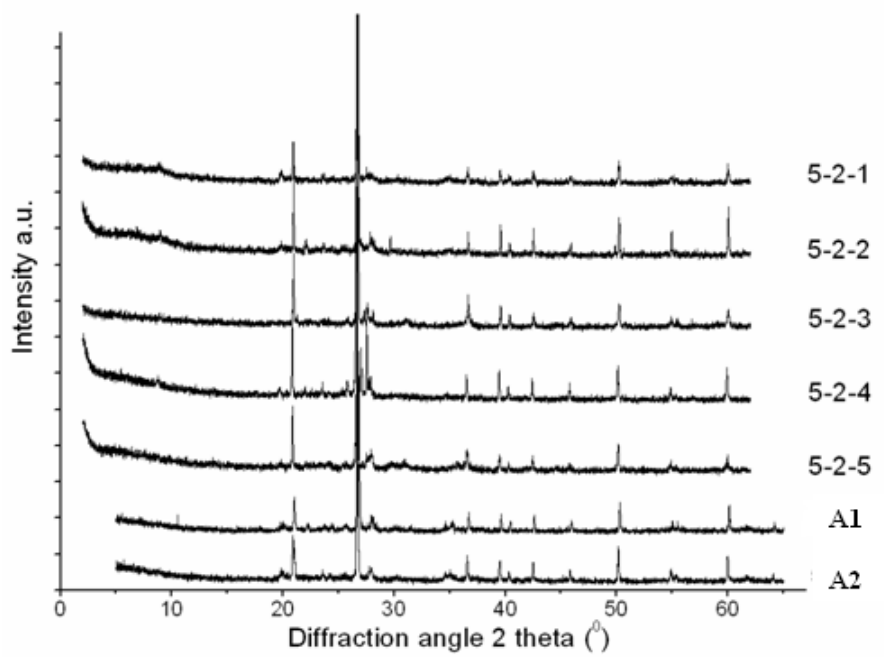

Figure 1. XRD patterns of the studied ceramic samples (5-2-1 to 5-2-5) and of two representative soil samples (A1, A2) (detailed diffractograms of the ceramics presented in [1])

The aim of this study is a more pertinent interpretation of the XRD and FT-IR results, with the aid of additionally derived (small yet significant) similarities or differences of the samples which eventually could lead to a proper classification of the items. This obviously necessitates further micro-structural (XRD) and compositional (XRD, FT-IR) characterization of the samples, starting from (and processing of) the XRD and FT-IR data formerly obtained. In case of multiphase samples, the detailed quantitative XRD crystal phase analysis may be achieved using the crystallites microstructural parameters extracted from the primary diffraction data, applying a Rietveld refinement routine and single X-ray diffraction line profile analysis. [6-8] The broad band generating overlapping FT-IR peaks assigned to the different mineral phases present can be identified by curve fitting deconvolution which mathematically enhances the resolution (without changing the experimental spectra), resolves the overlapped peaks, and allows the identification of the constituting mineral phases, offering a detailed qualitative and quantitative spectrum analysis. [9-12]

RESULTS AND DISCUSSION

Microstructural XRD analysis

XRD is increasingly used for the microstructural characterization of multiphase polycrystalline materials like geological samples or ceramics. [13-16] The position and shape (line broadening) of the experimental diffraction peak are both defined by the microstructure of the material. Peak shifts are related to internal stresses, peak broadenings, apart from that caused by instrumental imperfections, are sample-related: crystallites size distribution and micro-deformations (doping, isotropic or anisotropic micro-strains, stacking faults, etc.).

Microstructural characterization of the ceramic finds and the clayish soil samples collected was performed using the Rietveld method and XRD line profile analysis. [17-20] Experimental data are summarized in Table 1.

Table 1. Microstructural data of the ceramic shards and the soil samples

Sample	Microstructural data								
	V (nm^3)						Q		
	Bt	Mu_2	Mu_3	Orth.	M	Q	Unit-cell edges (nm)		D_{eff} (nm)
							a	c	
5-2-1	0.495	0.921	0.937	0.723	–	0.1126	0.4910	0.5404	124.6
5-2-2	0.492	0.934	0.934	0.725	–	0.1130	0.4914	0.5402	151.6
5-2-3	0.496	0.938	0.929	–	0.164	0.1132	0.4922	0.5396	167.7
5-2-4	0.502	0.938	0.933	–	0.167	0.1122	0.4893	0.5407	43.0
5-2-5	0.494	0.937	0.935	–	0.164	0.1132	0.4915	0.5409	44.1
A1									61.0
A2									63.7
Ref.*	0.498	0.938	0.935	0.725	0.168	0.1130	0.4913	0.5405	

Bt: biotite [3] 1M; Mu2: muscovite 2M(1); Mu3: muscovite [3] 2M(1);
Orth: orthoclase-type K-feldspar; M: mullite; Q: quartz.
*Reference values of AMCSD [21] and mindat.org [22] database.

The predominant mineral components of the ceramic matrix are quartz, (mainly K and some Na feldspars: orthoclase, plagioclase), variable amounts of phyllosilicates (mainly micas: muscovites, biotite) and minor quantities of heavy minerals (pyroxenes, iron oxides). [1] Quartz and feldspars probably play the role of the main temper materials of the clay paste.

Microstructural parameters of the SiO_2 crystallites contained by the ceramic samples were determined considering the α-quartz (100) and (200) XRD line profiles. The experimental unit-cell parameters (edge values *a*, *c*

and unit-cell volumes V) agree well with the AMCSD (American Mineralogist Crystal Structure Database) reference values. Unit-cell volumes for the main mineral components of the ceramic samples were also determined. The differences of the real V values and the mindat.org database reference values are in the experimental error limits in all cases.

Effective mean diameter D_{eff} of the quartz crystallites was determined for the ceramic samples and two of the soil samples collected, A1 and A2. According to the D_{eff} values obtained, the ceramics form three groups: (5-2-1), (5-2-2; 5-2-3), and (5-2-4; 5-2-5), suggesting three different raw material sources. The relative closeness of D_{eff} values found in the soil samples A1, A2 to those of the third ceramic group could indicate (at least in this case) a possible local provenance of the raw materials..

In multiphase samples the phase scattering cross-section for Bragg scattering is proportional to N/V, and N, the number of unit cells which contribute to the scattering, is proportional to I_R. [3] Accordingly, the quantitative phase analysis of the ceramics main mineral components was performed using the corresponding experimental unit-cell volume values, V (Table 1), and the relative peak intensities I_R data published before. [1] Abundance of the main mineral phases (vol%) is summarized in Table 2.

Table 2. Mineral composition of the ceramic samples
(main mineral phases only)

Sample	Mineral phases (vol%)					
	Bt	**Mu_2**	**Mu_3**	**Orth.**	**M**	**Q**
5-2-1	10.99	55.72	–	23.82	–	9.47
5-2-2	8.56	71.45	–	11.81	–	8.18
5-2-3	9.91	56.60	17.38	–	0.51	15.60
5-2-4	1.87	6.57	87.30	–	–	6.26
5-2-5	6.41	71.34	9.40	–	1.30	11.56

Bt: biotite; Mu_2.Mu_3: muscovites; Orth: orthoclase;
M: mullite; Q: quartz.

The values of Table 2 are in general accordance with the semi-quantitative values formerly published [1], with minor differences attributed to the samples overall heterogeneity, determined by the matrix texture, the presence and non-uniform distribution of the pores, of the non-plastic components (clasts) derived from pre-firing residual clay minerals or the applied temper, of newly formed firing minerals, and of post-burial alteration products. Ceramics heterogeneity is influenced, besides the composition of the green clay paste (determined by the raw materials), by the fabrication technology: the paste preparation method (use of levigated clays, with or without temper added), the firing temperature, kiln redox conditions.

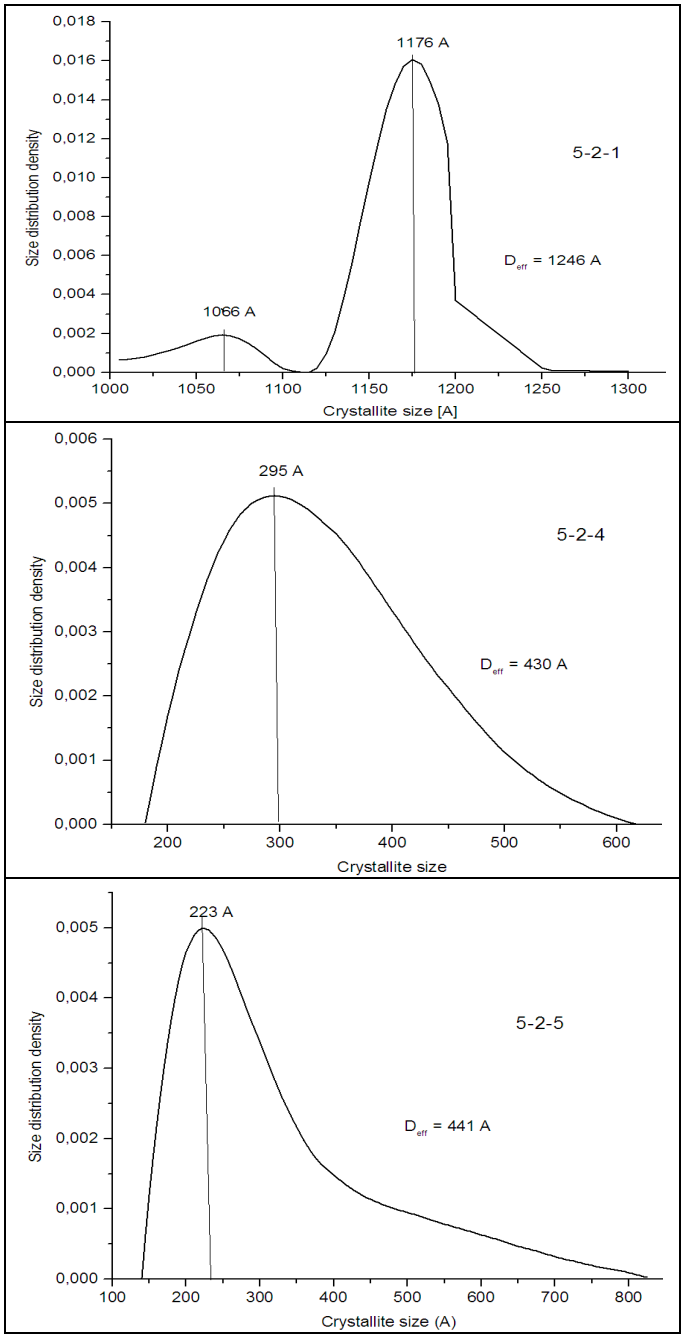

Figure 2. Probability distribution of quartz crystallites size in ceramic samples of hiatal (5-2-1) and serial (5-2-4, 5-2-5) fabric

The size distribution of the crystalline non-plastics characterize the crystalloclasts, added deliberately to the clay mixture as temper material,,or present a priori in the mixture's clay component(s). Typical crystalloclasts of the studied ceramics are quartz, micas, feldspars, and various heavy minerals, mostly iron oxides. [1] Size distribution probability of the most common (quartz) crystallites was determined with the Warren-Averbach XRD line profile analysis of the (100) and (200) SiO_2 quartz peaks, using the XRLINE computer program. [18] The patterns resulted for the 5-2-1, 5-2-4 and 5-2-5 samples are presented on Fig. 2.

The data obtained led to slightly different conclusions about the serial or hiatal character of the ceramic matrix fabric than the former OM results [1], suggesting that the correct interpretation require the knowledge of the similar data obtained for all the main crystalloclasts present in the ceramic system. However, the quartz crystallites size distribution probability curves (defined mainly by the sand naturally present in the green clay or used deliberately as temper) support the same sample grouping as the OM and respectively the D_{eff} data.

The quartz crystallites size distribution probability curves corresponding to the soil samples A1 and A2 were typical clayish soil grain size distribution diagrams. [21-24]

Table 2 data denotes that the amount of the main crystalline phases differ from sample to sample. Considering this and the fact that according the OM data the ceramics contain different types of heavy minerals [1], results that the raw clay(s) cannot have the same provenance. The type of the firing minerals formed and their XRD peaks relative intensity implies that the ceramics were fired in different conditions as well.

The great I_R values resulted for the quartz phase in every sample leads to the conclusion that the tempering of the clay paste was assured mostly by deliberately added alluvial sand.

FT-IR spectroscopy

Infrared spectroscopy is a sensitive tool to monitor the processes occurred during the firing, everyday use and burial of ancient ceramics, as well as to characterize the mineral composition and the (poorly or well) crystallized, sometimes partially glassy structure.

The broad OH bands appearing on the FT-IR spectra of the clayish materials around 3400 cm^{-1} and 1600 cm^{-1}, and the broad symmetry band centred around 1050 cm^{-1} are characteristic for all (more or less disordered) clay based systems. They are formed by overlapping (convolution) of the adjacent characteristic peaks of the constituting minerals. The OH bands

are frequently weakened, or even absent, as their intensity depends, besides the ceramic composition and structural compactness, on the firing conditions and the re-hydration processes taking place during burial, the later being determined by the environmental conditions,. The band around 1050 cm^{-1} characterizes the connectivity of the Si–O, Al–O and Si–O–Al units, being closely related to the structural ordering of the ceramics. [9-11]

Deconvolution of the broad bands can help to differentiate between the ceramic samples, because the constituting mineral phases can be identified through the relative intensities of the –OH, Si–O, Al–O and Si–O–Al units stretching and bending modes. However, the spectral component set is not unequivocal, and attribution (assignment) makes sense only for parent materials belonging to the same or contiguous families. [10] In conclusion, the component bands positions (given by the parameter w), and intensity (given by A), determined using the Origin 8 software (Fourier Self-Deconvolution, FSD), always imply a certain degree of subjectivity. [25] The overall reliability of the deconvolution process in this specific case, is satisfactory, as the basic criteria necessary to be fulfilled in order to consider an acceptable curve-fitting were accomplished (Table 3). The lowest χ^2 (RMS, root-mean-square) values required for good results were reached. (acceptable RMS values has to be of magnitude 10^{-5} for spectra with maximum absorbance values in the 0.05-0.09 range); the below and above fits converge on the same model; the second derivative of the composite sums overlies the second derivative of the original spectra.

Spectral deconvolution of the main peaks of sample 5-2-2, realized by the Gaussian peak-shape function method, is presented on Fig. 3.

As in this case the best goodness-of-fit, measured by the χ^2 parameter, was obtained with a pure Gaussian function, spectral deconvolution was realized using the Gauss profile, taking into account, based on the literature data, the corresponding number of components for each spectral massif. The deconvoluted peaks' absorption frequencies were assigned considering the literature data corresponding to the most common clay minerals and to the previous data obtained on ancient ceramic samples (Table 4). [9-12, 25-39] Since – as exemplified by Fig. 3 for the sample 5-2-2 - the shape of the spectral patterns modelled by the convolution of the calculated absorption bands fit well the experimental spectra, the model can be accepted as correct.

Infrared spectroscopy closely monitors the thermal processes (dehydroxylation, dehydration, redox transformations) taking place during the firing of clay minerals. [40] In this case the weakness or the absence of OH bands and the presence of broad symmetry band centered around 1050 cm^{-1} means that the samples have been fired above 600^0C and were made of a mixture of at least two disordered clays. The presence of iron oxides also confirms the firing temperature as above 600^0C. Prominent peaks at ≈500 cm^{-1} reveals that even if the sample was fired under reduced

atmosphere, air has been allowed at a higher temperature during the cooling, enabling the oxidation of iron components (allowing air during cooling being a common practice for coloration in red of the baked clays). Sandwich structure also indicates firing under reduced atmosphere and admission of the air only at the lower temperature of the cooling.

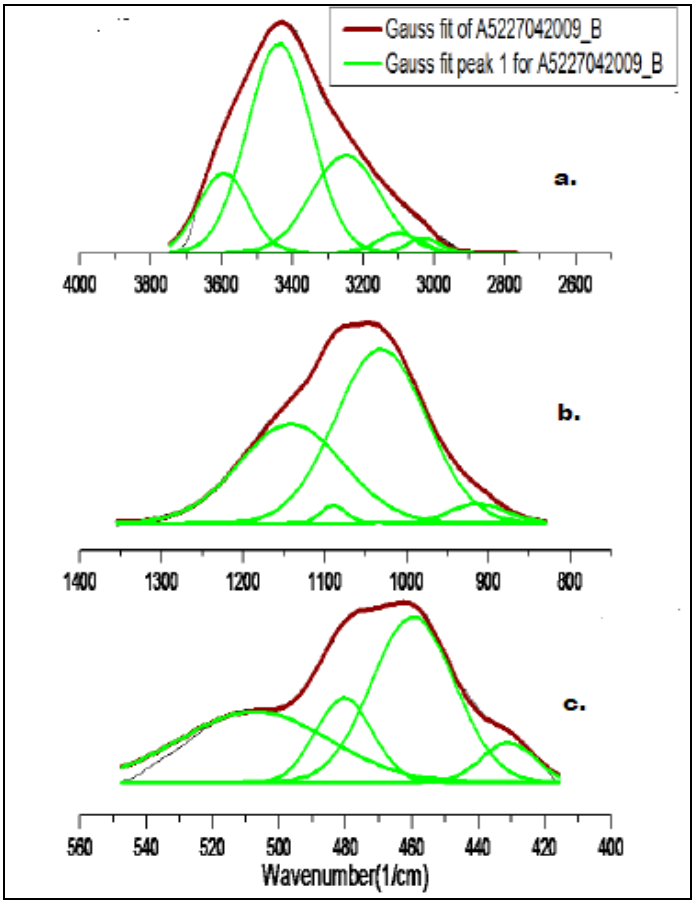

Figure 3. FT-IR spectrum deconvolution for the sample 5-2-2.
Spectral regions: (a) 3800-2800 cm^{-1} (b) 1500-800 cm^{-1}, (c) 600-400 cm^{-1}.

Table 3. FT-IR deconvolution data of the ceramic samples. Resolved bands: 3600-3000 cm^{-1} (O-H band); 1300-850 cm^{-1} (main Si-O / Al-O / Si-O-Al band); 600-400 cm^{-1} (Al-O. Si-O-Al. Si-O-Me. Al-O-Me band). w – peak wavenumber (cm^{-1}); A – peak area

Spectral region	Ceramic sample									
	5-2-1		5-2-2		5-2-3		5-2-4		5-2-5	
	w	A	w	A	w	A	w	A	w	A
3600-3000 cm^{-1}			3595	6.9						
	3568	20.0					3568	7.2	3568	6.2
	3435	40.0	3438	30.0			3435	12.0	3435	7.1
	3290	30.0					3291	9.0	3290	7.5
			3250	15.0						
	3103	12.0	3100	1.8			3103	3.3	3103	3.6
			3030	1.0						
	2940	1.8					2940	0.4	2940	0.4
	2850	1.0					2850	0.1	2850	0.1
χ^2	0.00002		0.00002				0.00002		0.000006	
R^2	0.99737		0.99281				0.99746		0.99814	
1300-850 cm^{-1}									1246	10.0
	1164	44.6			1170	43.8			1158	23.0
			1142	61.6						
							1110	122.		
	1090	3.6	1090	2.6	1084	11.4	1086	5.8	1079	32.5
	1043	164.8	1032	95.1	1054	107.7				
							1012	40.2	990	55.0
	911	5.2	913	6.4			916	5.9		
χ^2	0.00004		0.00003		0.00005		0.0001		0.00013	
R^2	0.9997		0.99957		0.99937		0.99847		0.99487	
600-400 cm^{-1}									513	0.4
	501	12.5	508	6.0	509	7.2	505	4.5		
	481	3.8	480	2.7	483	2.5	478	3.8	483	4.0
	461	10.0	460	7.8	461	16.0	460	2.7	457	5.5
							448	10.0		
	433	4.0	431	1.2	428	2.5			427	1.2
χ^2	0.00003		0.00006		0.00004		0.00006		0.00001	
R^2	0.99847		0.99207		0.99799		0.99397		0.99605	

Table 4. FT-IR deconvolution data of the ceramic samples.
The resolved bands attribution [[9, 10, 27-39].

Wavenumber cm^{-1}	Tentative assignment	Species associated
Spectral domain 3600-3000 cm^{-1}		
3595	O–H str	mica (Na-vermiculite)
3568		mica (Mg-vermiculite)
3438-3435	adsorbed water	montmorillonite, chlorite
3290-3291	N–H str	organic matter remains
3250		
3103-3100	C-H str	organic remains (methyl and methylene sym. and asym. stretching)
3030		
2950		
2840		
Spectral domain 1300-850 cm^{-1}		
1246	C–O str asym. phosphate str	CO_3^{2-} (sample weathering) bone remains (?)
1170-1158	Si–O str	quartz
1142	Si–O/Al–O–Si/O–Si–O str.	quartz, aluminosilicates (kaolinite, illite, smectite, metasmectite)
1110		
1090-1079		
1054-1032		
1012-990	Si-O str.; O–H deform.	kaolinite
918-911	Al–O–H str.; O–H deform.	
Spectral domain 600-400 cm^{-1}		
509-501	Si-O-Al / Fe-O bending	octahedral Al, hematite
483-478	Si–O–Si bending	silicates
461-457		
448	Si–O deform	
433-427		

FT-IR absorption results confirm the mineralogical data obtained by polarized light microscopy and by XRD. The deconvolution results of the 3400 cm^{-1} centered large O-H absorption band, of that of the 1100 cm^{-1} centered Si-O-Si band, and that of the 460 cm^{-1} centered Si-O / Al-O / Si-O-Al band indicate – in concordance with the XRD data - the distinct raw material source (different provenance) of the ceramic samples, as well as their different firing conditions (different fabrication technologies).

CONCLUSIONS

The experimental unit-cell parameters of the SiO_2 crystallites determined by the α-quartz (100) and (200) XRD line profile analysis agree well with the AMCSD (American Mineralogist Crystal Structure Database) reference values. The differences of the real V unit-cell volumes' values determined for the main mineral components of the ceramic samples and the mindat.org database reference values are in the experimental error limits in all cases.

According the effective mean diameter D_{eff} values obtained, the ceramic samples form three groups: (5-2-1), (5-2-2; 5-2-3), and (5-2-4; 5-2-5), suggesting three different raw material sources. The relative closeness of the D_{eff} values of the soil samples A1 and A2 (recolted nearby the archaeological site) to those of the third ceramic group, could suggest a possible local provenance of the raw materials in this case.

The quantitative phase abundance of the ceramics' main mineral components determined using the experimental unit-cell volume values V and the relative peak intensities I_R data published before [1] is in general accordance with the former semi-quantitative values [1], with minor differences which can be attributed to the samples overall heterogeneity, characteristic for archaeological ceramics.

The size distribution data of the quartz crystallites (the most common crystalloclasts) led to slightly different conclusions about the serial or hiatal character of the ceramic matrix fabric than the former OM results [1], suggesting the necessity of the knowledge of the similar data for all the main crystalloclasts present in the ceramic system. However, the size distribution probability patterns confirm the sample grouping resulted from OM and D_{eff} data.

Considering that the amount of the main crystalline phases and the heavy minerals contained by the different samples [1] differ, the raw clay(s) cannot have the same provenance. As the type and abundance of the firing minerals formed also differ, the ceramic technology (firing conditions) differ as well, excepting that (as results from the great I_R values of the quartz phase in every sample) the tempering of the clay paste might be assured by deliberately added alluvial sand.

The weakness or the absence of OH bands and the presence of broad symmetry band centered around 1050 cm^{-1} means that the ceramic samples, made from the mixture of at least two disordered clays, have been fired above 600^0C. The presence of iron oxides also confirms the firing temperature as above 600^0C. Prominent peaks at ≈500 cm^{-1} reveals that even if the sample was fired under reduced atmosphere, air has been allowed at a relatively higher temperature during the cooling, enabling the oxidation of iron components. Sandwich structure observed in the case of sample 5-2-2 [1] also indicates firing under reduced atmosphere and admission of the air during the cooling.

FT-IR absorption results confirm the mineralogical data obtained by other methods. The deconvolution results indicate, in concordance with the microstructural XRD data, different raw material sources and different fabrication technologies (firing conditions) of the ceramic samples.

EXPERIMENTAL SECTION

The powder XRD patterns were obtained as presented before. [1] Unit cell parameters were calculated through Rietveld refinement using the PowderCell software [17-19, 41]. The crystalline phase composition was determined using the MATCH! Phase Identification from Powder Diffraction software together with the "IUCr/COD/AMCSD" reference database [42, 43]. Microstructural informations referring to the SiO_2 crystallites contained in the samples were obtained by Warren-Averbach single X-ray profile analysis [17-19] of the (100) and (200) SiO_2 quartz peak profiles processed by the XRLINE computer program [18].

FT-IR sample preparation and spectra recording were as described in [1]. Deconvolution of the IR absorption bands corresponding to the OH and the SiO (AlO) regions, respectively, was performed using the Origin 8 Pro data analysis software.

ACKNOWLEDGEMENTS

The presented work is partly supported by the research project entitled "Transylvanian technical and cultural legacy. Industrial archaeology, archaeometallurgy and archaeometry" started by the Science and Engineering Department of the Research Institute of the Transylvanian Museum Society.

Our special thanks to Dr. Viorel Ciubotă and Róbert Gindele from the Satu Mare County Historical Museum for entrusting the samples.

REFERENCES

1. E. Bitay, B. Kiss-Pataki, Gy. Szakmány, E. Indrea, I. Kacsó, I. Bratu, E. Veress, *Studia UBB Chemia*, **2017**, *62*, 4/1, 155.
2. G. Eramo, M. Maggetti, *Applied Clay Science* **2013**, *82*, 16-23.
3. M. Emami, Y. Sakali, C. Pritzel, R. Trettin, *Journal of Microscopy and Ultrastructure* **2016**, *4*, 1, 11.
4. C. Rathossi, V. Pontikes, *Journal of the European Ceramic Society*, **2010**; *30*, 9, 1841-1851

5. M.I Dias, A.C Valera, M.I. Prudêncio, *Proceedings of EMAC'03 "Understanding People through their Pottery",* A. Marques de Faria, Ed., *Trabalhos de Arqueologia*, **2005**, *42*, 41.
6. C.T. Kniess, J.C. de Lima, P.B. Prates, *Sintering-Methods and Products*., V. Shatokha, Ed., ISBN: 978-953-51-0371-4, InTech, **2012**, 293
7. R. Martineau, A.V. Walter-Simonnet, B. Grobéty, M. Buatier, *Archaeometry,* **2007**, *49*, 1, 23.
8. G. Barone, L. Bartoli, C.M. Belfiore, V. Crupi, F. Longo, D. Majolino, P. Mazzoleni, V. Venuti, *Journal of Analytical Atomic Spectrometry*, **2011**, *26*, 5, 1060.
9. D. Barilaro, V. Crupi, S. Interdonato, F. Longo, G. Maisano, D. Majolino, V. Venuti, G. Barone, P. Mazzoleni, G. Tigano, S. Imberti, *Il Nuovo cimento della Società italiana di fisica. C*, 31(3), **2008**, 371.
10. S. Shoval, Y. Paz, *Periodico di Mineralogia*, **2015**, *84*, 213.
11. C.I. Fialips, D. Huo, L. Yan, J. Wu, J.W. Stucki, *Clays and Clay minerals*, **2002**, *50*, 4, 455-469.
12. Ph. Colomban, *RSC Analytical Spectroscopy Monographs Vol. 9*, H.G. Edwards and J.M. Chalmers, Eds., Royal Society of Chemistry, **2005**, 192.
13. V. Simić, P. Uhlík, *Geoloski anali Balkanskoga poluostrva*, **2006**, *67*, 109.
14. T. Ungár, P. Martinetto, G. Ribárik, E. Dooryhee, P. Walter, M. Anne, *Molecular and Structural Archaeology: Cosmetic and Therapeutic Chemicals*, G. Tsoucaris, J. Lipkowski, J., Eds., Springer, Dordrecht, **2003**, 211.
15. E. Schafler, M. Zehetbauer, *Reviews on Advanced Materials Science*, **2005**, *10*, 28.
16. T. Ungár, J. Gubicza, *Zeitschrift für Kristallographie-Crystalline Materials*, **2007**, *222*, 3-4, 114.
17. H. Rietveld, *Journal of Applied Crystallography*, **1969**, *2*, 2, 65.
18. N. Aldea E. Indrea, *Computer Physics Communications*, **1990**, *60,* 1, 155.
19. J.G. Van Berkum. A.C. Vermeulen, R. Delhez, T.H. de Keijser, E.J. Mittemeijer, *Journal of applied crystallography*. **1994**, 27, *3,* 345.
20. G.M. Hansford, S.M.R. Turner, P. Degryse, A.J. Shortland, *Acta Crystallographica, A: Foundations and Advances*, **2017**, *73*, 4, 293.
21. R.T. Downs, M. Hall-Wallace, *American Mineralogist*, **2003**, *88*, 1, 247.
22. The Hudson Institute of Mineralogy Database (Mindat.org).
23. G. Cultrone, C. Rodriguez-Navarro, E. Sebastian, O. Cazalla, M.J. De La Torre, *European Journal of Mineralogy*, **2001**, *13*, 3, 621.
24. D.P. Braun, *Journal of Field Archaeology*, **1982**, *9*, 2, 183.
25. S. Roberta, R. Gaetano, J.H. Robin, A.M. De Francesco, *Mediterranean Archaeology & Archaeometry*, **2017**, *17*, 2, 1.
26. M. Hardy, *Clay Minerals*, **1992**, *27*, 1, 47.
27. A. Tinti, V. Tugnoli, S. Bonora, O. Francioso, *Journal of Central European Agriculture*, **2015**, *16*, 1, 1.
28. P. Djomgoue, D. Njopwouo, FT-IR spectroscopy applied for surface clays characterization. *Journal of Surface Engineered Materials and Advanced Technology*, **2013**, *3*, 04, 275.
29. D. Seetha, G. Velraj, *Journal of applied research and technology*, **2016**, *14*, 5, 345.

30. R. Palanivel, U.R. Kumar, *Romanian Journal of Physics*, **2011**, *56*, 1-2, 195.
31. P. Sathya, G. Velraj, *Journal of Experimental* Sciences, **2011**, *2*, 5, 04.
32. T.F.M. Oudemans, J.J. Boon, R.E. Botto, *Archaeometry*, **2007**, *49*, 3, 571.
33. A. Dazzi, C.B. Prater, *Chemical reviews*, **2016**, *117*, 7, 5146.
34. S. Dallongeville, N. Garnier, C. Rolando, C. Tokarski, *Chemical reviews*, **2015**, *116*, 1, 2.
35. L. Bachmann, R. Diebolder, R. Hibst, D.M. Zezell, *Spectrochimica Acta, A: Molecular and Biomolecular Spectroscopy*, **2005**, *61*, 11-12, 2634.
36. G. Ricci, L. Caneve, D. Pedron, N. Holesch, E. Zendri, *Microchemical Journal*, **2016**, *126*, 104.
37. M. Diko, G. Ekosse, J. Ogola, *Acta Geodynamica and Geomaterialia*, **2016**, *13*, 2, 149.
38. P. Sathya, G. Velraj, S. Meyvel, *Advances in Applied Science Research*, **2012**, *3*, 2, 776.
39. L. Vaculikova, E. Plevova, S. Vallova, I. Koutnik, *Acta Geodynamica et Geomaterialia*, **2011**, *8*, 1, 59.
40. G.E. De Benedetto, R. Laviano, L. Sabbatini, P.G Zambonin, *Journal of Cultural Heritage*, **2002**, *3*, 3, 177.
41. G. Nolze, PowderCell: A mixture between crystal structure visualizer, simulation and refinement tool. *Powder Diffraction: Proceedings of the II International School on Powder Diffraction*, **2002**, 146.
42. http://www.crystalimpact.com/match/
43. T.T. Downs, M. Hall-Wallace, *American Mineralogist* **2003**, *88*, 247.